Oscillating Electric Fields in Liquids Create a Long-Range Steady Field

Aref Hashemi, Scott C. Bukosky, Sean P. Rader, William D. Ristenpart,* and Gregory H. Miller†
Department of Chemical Engineering, University of California Davis, Davis, California 95616, USA

(Received 6 April 2018; revised manuscript received 19 July 2018; published 2 November 2018)

We demonstrate that application of an oscillatory electric field to a liquid yields a long-range steady field, provided the ions present have unequal mobilities. The main physics is illustrated by a two-ion harmonic oscillator, yielding an asymmetric rectified field whose time average scales as the square of the applied field strength. Computations of the fully nonlinear electrokinetic model corroborate the two-ion model and further demonstrate that steady fields extend over large distances between two electrodes. Experimental measurements of the levitation height of micron-scale colloids versus applied frequency accord with the numerical predictions. The heretofore unsuspected existence of a long-range steady field helps explain several long-standing questions regarding the behavior of particles and electrically induced fluid flows in response to oscillatory potentials.

DOI: 10.1103/PhysRevLett.121.185504

Many systems of practical and scientific importance involve application of an oscillatory electric potential to a liquid, including dielectric and impedance spectroscopy [1–3], cyclic voltammetry [4,5], electroacoustics [6,7], dielectrophoresis [8,9], induced charge electrokinetics [10–13], and electrohydrodynamic manipulation of colloids [14–18]. In contrast to perfect dielectrics, the presence of mobile ions in the liquid phase complicates interpretation of the electric field. The "standard electrokinetic model" [19,20] is a continuum level model widely used to predict the behavior of charged ions in solution. It couples Gauss's law for the electric potential with the Nernst-Planck conservation equations for each ionic species, yielding a system of nonlinear coupled differential equations. For most systems of interest, the model is characterized by extremely sharp gradients in the non-electroneutral ionic charge layer near any solid or liquid interfaces [21]. Accordingly, most theoretical and numerical analyses of the standard electrokinetic model have focused on asymptotic solutions in the limit of small applied potentials [1,20,22,23], which, for sinusoidal applied potentials, invariably yield a sinusoidal electric field inside the liquid, albeit with phase lag and amplitude that depend on the system properties.

Importantly, these linearized asymptotic solutions differ qualitatively from recent numerical computations of the fully nonlinear electrokinetic model by Olesen *et al.*, who found that the electric field assumes a much more complicated shape at sufficiently high applied oscillatory potentials [24]. This finding, which was further corroborated analytically by Stout and Khair [25] and Schnitzer and Yariv [26], is significant because analyses of the behavior of individual colloids or other objects in liquids typically begin with the assumption that the electric field is perfectly sinusoidal, and it is unclear what the influence of a nonsinusoidal field will be. Further complicating matters, the prior nonlinear analyses [24–26] restricted attention to situations where the ionic mobilities of the positive and negative ions were equal, which simplifies the analysis but rarely pertains to actual liquids.

To consider the effect of nonequal ionic mobilities, first, we introduce a two-ion model that illustrates how an ionic mobility mismatch can yield a steady field nearby (Fig. 1). Consider two isolated ions with charge numbers q_+ and q_-, respectively, each oscillating in response to a one-dimensional far-field sinusoidal electric field of magnitude $E_0 \cos(\omega t)$. The ions are treated as noninteracting points (consistent with the continuum approximation) but with mobilities that differ based on their drag coefficients in liquid with viscosity μ. Neglecting inertia and balancing the drag force with the electrostatic driving force yields

$$6\pi\mu a_i \frac{dz_i}{dt} - q_i e E_0 \cos(\omega t) = 0, \tag{1}$$

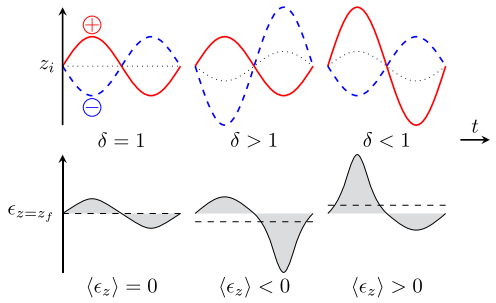

FIG. 1. Two-ion harmonic oscillator model. (Top) Harmonic trajectories of two ions moving in response to a far-field sinusoidal electric field, for different ionic mobility ratios. (Bottom) Corresponding perturbation to the electric field evaluated at $z = z_f$.

where z_i denotes the instantaneous location of ion i with size a_i. Solving for the position yields

$$z_i = \frac{q_i e E_0}{\omega(6\pi\mu a_i)} \sin(\omega t). \tag{2}$$

The obtained harmonic oscillators of the ions $z_i(t)$ are shown schematically in Fig. 1, where $\delta = a_+/a_-$ is taken as a measure for the ionic mobility mismatch. For $\delta = 1$, ions oscillate with the same amplitude and the center of charge remains stationary. However, when $\delta \neq 1$, the fast moving ion exhibits a higher amplitude compared to the slow moving one, causing the center of charge itself to oscillate.

Now, we ask what happens at a point $z = z_f$ far from the ions due to their harmonic oscillation. Expansion of Coulomb's law in a Taylor series for $z_i/z_f \to 0$, followed by substitution of the harmonic solutions of Eq. (2) and rearrangement, yields the perturbed electric field

$$\epsilon(z_f, t) = \frac{\alpha}{z_f^2}[2\hat{E}(1+\delta)\sin(\omega t) + 3\hat{E}^2(1-\delta^2)\sin^2(\omega t) + 4\hat{E}^3(1+\delta^3)\sin^3(\omega t) + \ldots], \tag{3}$$

where $\hat{E} = eE_0/(6\pi\mu a_+ \omega z_f)$ and $\alpha = e/(4\pi\varepsilon_\infty\varepsilon_0)$. (See Supplemental Material [27] for full derivation.) The observed electric field versus time is multimodal with frequency peaks at odd integer multiples of the imposed frequency for ions with $\delta = 1$, but with frequency peaks at both odd and even integer multiples of the imposed frequency for $\delta \neq 1$. This mobility dependence has an important consequence for the time average of the perturbation field near the oscillating ions. Integrating Eq. (3) yields the time average, to leading order,

$$\langle \epsilon(z_f) \rangle = \frac{\omega}{2\pi} \int_0^{2\pi/\omega} \epsilon(z_f, t) dt = \frac{3\alpha\hat{E}^2(1-\delta^2)}{2z_f^2}. \tag{4}$$

Provided $\delta \neq 1$, there is a nonzero time-average electric field due to the uneven oscillation of the ions. This phenomenon, which we denote as an "asymmetric rectified electric field" (AREF), is depicted graphically along the bottom of Fig. 1. The perturbation to the net electric field at a location z_f is dominated by the faster moving ion, since it will be in closer proximity than the slower moving ion. This imbalance yields a net electric field that, to leading order, scales as the square of the applied field strength.

The preceding toy model is suggestive, but it omits ion-ion interactions and the influence of thermal energy (i.e., diffusive motion). To capture these effects, one must invoke the standard electrokinetic model. For simplicity, here, we focus on the one-dimensional electric field between parallel electrodes separated by a distance H. The liquid contains two ionic species, each with concentration n_i and diffusivity $D_i = k_B T/(6\pi\mu a_i)$, which defines the ionic mobility mismatch $\delta = D_-/D_+$. The standard electrokinetic model couples Gauss's law

$$\varepsilon_\infty\varepsilon_0 \frac{\partial^2\phi}{\partial z^2} = -\sum_{i=1}^{2} e q_i n_i, \tag{5}$$

with Nernst-Planck continuity equations for each ionic species

$$\frac{\partial n_i}{\partial t} = D_i \frac{\partial^2 n_i}{\partial z^2} + e q_i \frac{D_i}{k_B T} \frac{\partial}{\partial z}\left(n_i \frac{\partial\phi}{\partial z}\right). \tag{6}$$

The first and second terms on the right-hand side of Eq. (6) describe the ion diffusive motion and the electromigration in response to the local electric field, respectively. To complete the problem statement, we impose an oscillatory electric potential of amplitude ϕ_0 and frequency $f = \omega/(2\pi)$ on the lower electrode at $z = 0$, while keeping the upper electrode grounded. We further impose no flux of ions through each electrode; i.e., the electrodes are "blocking" and do not permit any electrochemical reactions. This assumption might not pertain for sufficiently large applied potentials; here, we focus on the limiting case of negligible electrochemistry.

We emphasize that Eqs. (5) and (6) are the classical starting point for analysis of the electrical behavior of fluids with ionic charge. In contrast to prior work, however, here, we make no assumptions about the magnitude of the applied sinusoidal potential, nor about the values of the ionic mobilities. The system of equations was solved via finite difference methods with mesh refinement to capture the extremely thin Debye layers (~10 nm) near the boundaries (see Supplemental Material [27]).

Examining the case of equal ionic mobilities ($\delta = 1$) first, the electric field varies sinusoidally versus time for sufficiently low applied potentials [black curve, Fig. 2(a) ($\phi_0 e/(k_B T) = 1$)], with magnitude and phase lag as predicted by the linearized analytical solution ([1] and Fig. S2 [27]). As the voltage increases, the contributions of the nonlinear terms yield increasingly large multimodal peaks, a behavior that linearized models fail to predict. Qualitatively similar multimodal peaks were found previously [24–26], but here, our numerics show that the multimodal peaks occur precisely at odd integer multiples of the imposed frequency, consistent with the two-ion model [cf. Eq. (3) and Fig. S3 [27]]. Note that the observed left-right asymmetry of the harmonic solution is a direct result of this multimodal behavior. In the case of nonequal mobilities [Fig. 2(b)], for sufficiently low applied potential, the electric field is again a simple sinusoid versus time, and multimodal peaks grow in magnitude as the applied potential increases. Unlike the case of equal mobilities, however, for $\delta = 4$, the shape of the electric field versus time is substantially shifted, with multimodal peaks

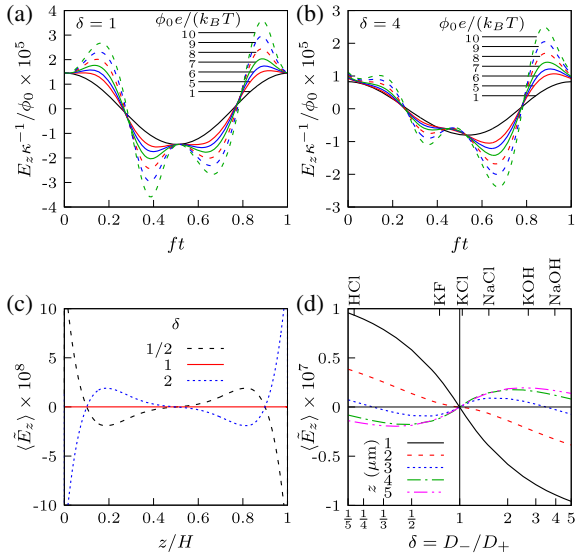

FIG. 2. Effects of applied voltage and ionic mobility mismatch on the electric field between parallel electrodes. (a) and (b) Harmonic solutions of the normalized electric field $E_z\kappa^{-1}/\phi_0$ at $z = 1$ μm ($z/H = 0.04$) for different applied voltages: (a) $\delta = 1$, (b) $\delta = 4$. (c) Dimensionless time average electric field $\tilde{E}_z = E_z e\kappa^{-1}/(k_B T)$ versus z for different δ values. (d) Dimensionless time average electric field versus δ value at different locations. Parameters: $\phi_0 = 5k_B T/e$ (c) and (d), $f = 50$ Hz, $H = 25$ μm, $\min[D_+, D_-] = 1 \times 10^{-9}$ m^2/s, $c_\infty = 1$ mM.

occurring at both odd and even integer multiples of the imposed frequency.

Numerical integration of the electric field to obtain the time-average [cf. Eq. (4)] confirms that AREFs occur over large length scales across the entire domain [Fig. 2(c)]. For $\delta = 1$, the time average is identically zero everywhere [solid red curve, Fig. 2(c)]. In contrast, for $\delta = 2$ [dotted blue line, Fig. 2(c)], the time average electric field steeply rises from negative values near $z/H = 0$, passes through zero and reaches a maximum near $z/H = 0.2$, before decaying to identically zero at $z/H = 0.5$. The negative mirror image of this functionality occurs for $z/H > 0.5$; i.e., the AREF is antisymmetric with respect to position around $z/H = 0.5$. For the case of $\delta = 1/2$ [dashed black line, Fig. 2(c)], the AREF has the same magnitude but opposite sign everywhere as for the case of $\delta = 2$. The long-range steady field results from the uneven oscillation of the cations and anions, resulting in an augmentation or depletion of charge across the domain, provided $\delta \neq 1$ (Figs. S6 and S7 [27]). Numerical calculations over a wide range of values of δ confirm that the antisymmetric shape of the AREF is robust, and further demonstrate that the magnitude of the AREF increases with the difference between δ and unity [Fig. 2(d)]. We emphasize that the symmetry in the system is broken by the ionic mobility mismatch, not the relative orientation of the electrodes; the magnitude and sign of the AREF are independent of which electrode is powered or grounded. In other words, near each electrode the AREF is directed toward the electrode for $\delta > 1$, but away from the electrode for $\delta < 1$.

Perhaps a surprising aspect of the results shown in Figs. 2(c) and 2(d) is that the AREF occurs over such long length scales, well outside of the Debye layers (located here approximately at $z/H < 0.0004$ and $z/H > 0.9996$ for Debye length of 10 nm). Systematic calculations of the AREF over a range of applied field strengths and frequencies confirm that this long-range behavior occurs over a wide range of parameter space (Fig. 3). As the applied sinusoidal potential increases [Fig. 3(a)], the shape of the AREF versus position is conserved (i.e., the curves collapse), but its magnitude increases as the 1.9 power of the local peak-to-peak electric field, defined here as $E_{pp}(z) = \max[E_z(z,t)] - \min[E_z(z,t)]$. This behavior is consistent with the quadratic dependence predicted by the two-ion model [cf. Eq. (4)]; the slight discrepancy is presumably due to the more complicated shape of the actual local electric field [cf. Fig. 2(b)] compared to the simple sinusoid considered in the two-ion model. In contrast, the effect of frequency is more complicated [Fig. 3(b)]. At very low imposed frequencies, the AREF is small in magnitude but peaks at locations relatively far from the electrodes. As the frequency increases, the peak magnitude increases sharply, scaling as $\omega^{1.4}$, while the peak location shifts closer to the electrode, scaling as $\omega^{-0.5}$. Similarly, Fig. S5(a) [27] shows that the position of the peak AREF outside the Debye layer scales as the square root of the diffusivity. Taken together, these observations indicate that the characteristic length for AREFs outside the Debye layer scales as $L/H \sim \sqrt{D/(\omega H^2)}$. As the frequency increases, and this characteristic length scale decreases, there are an increasing number of positions where the AREF reverses direction. At low frequencies, the AREF only changes direction once before the midplane [cf. Fig. 2(c)], but at higher frequencies, it changes direction multiple times [cf. green curve in Fig. 3(b) ($f = 500$ Hz)].

The existence of a long-range steady field has significant implications for the behavior of colloids and electrically driven flows at the microscale. Even for a relatively small applied potential of 0.5 V, applied at 100 Hz in water with $\delta = 4$, the AREF-induced electrophoretic force on a 1-μm particle at $z = 1$ μm is a factor of 10^3 to 10^5 larger than the Brownian, gravitational, and dielectrophoretic forces acting on it (Table S1 [27]). A key experimental prediction, then, is that a particle placed between parallel electrodes will levitate upward against gravity provided the ions present have a sufficiently large mobility mismatch.

Indeed, recent work [32,33] has established that oscillatory fields do cause microscale colloids in millimolar NaOH ($\delta = 3.96$) to levitate many particle diameters upward against gravity, while the same particles in millimolar KCl ($\delta = 1.04$) do not. The mechanism for this levitation has been obscure, but the behavior is consistent with our AREF hypothesis: the long-range steady field

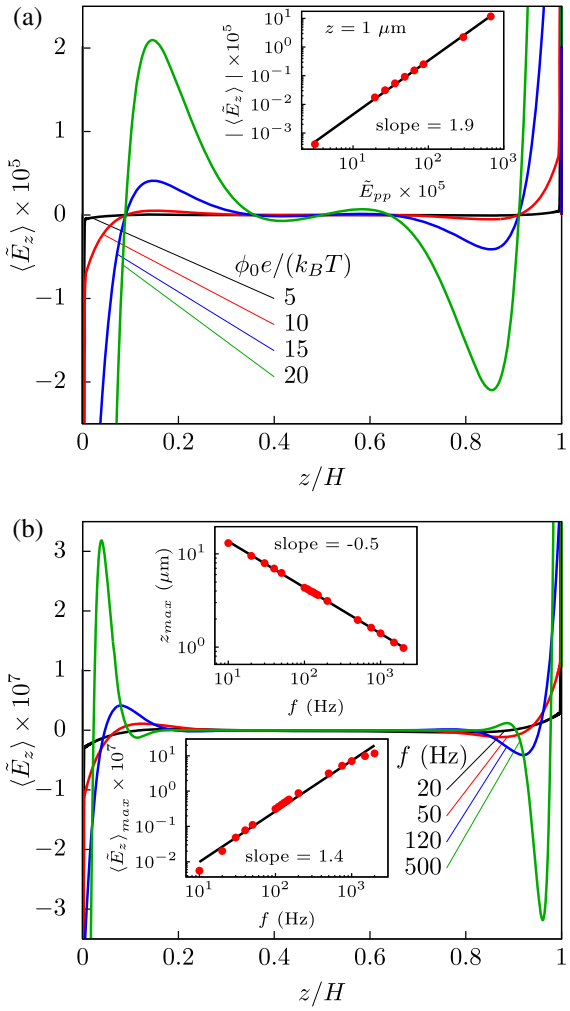

FIG. 3. Effects of voltage and frequency on the AREF. Distribution of the dimensionless time average electric field for different voltages (a) and frequencies (b). Parameters: $\phi_0 = 5k_BT/e$ (b), $f = 100$ Hz (a), $H = 25$ μm (a) and 50 μm (b), $\delta = 4$, $D_+ = 1 \times 10^{-9}$ m^2/s (a) and 1.3×10^{-9} m^2/s (b), $c_\infty = 1$ mM.

causes the particles to move upward until the AREF magnitude diminishes sufficiently for the electrophoretic force to balance with gravity. The complicated spatial dependence of the AREF also explains why some particles were observed to move upward against gravity, while others moved downward [32,33]. Note in Fig. 3(a) that the AREF is negative for $z/H < 0.1$, but positive for $0.1 < z/H < 0.35$; the direction of motion depends on the initial particle position (Fig. S8 [27]). Our additional experiments reveal that the levitation height scales with frequency precisely as $h \propto \omega^{-0.5}$ [(Fig. 4(b)], in accord with the frequency dependence predicted numerically [cf. Fig. 3(b)]. Simultaneously, the magnitude of the applied voltage had little impact on the levitation height [Fig. 4(c)], again in accord with the numerical predictions [Fig. 3(a)]. These observations provide strong experimental

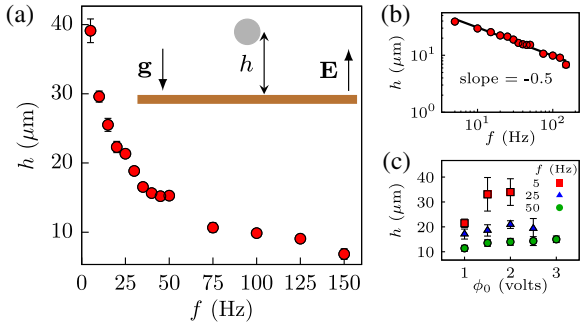

FIG. 4. Experimental evidence for AREFs: colloids levitating against gravity in response to an oscillatory field. (a) and (b) Stable levitation height versus frequency for 2-μm diameter polystyrene particles in 1 mM NaOH with a 4 V applied potential. (c) Levitation height versus applied potential at different frequencies. See Supplemental Material [27] for details.

evidence for the existence of AREFs in response to oscillatory potentials.

A previously unrecognized driving force of this magnitude will necessitate reconsideration of prior experimental studies involving oscillatory fields; here, we note two other systems of interest where AREFs help resolve outstanding questions. First, there has been long-standing controversy regarding the aggregation of micron-scale particles near electrodes in response to oscillatory fields. Early workers [14–16] established that colloids aggregated laterally near the electrode, in the direction perpendicular to the applied field, and attributed the aggregation due to electrohydrodynamic (EHD) flows generated on the electrode surface near each particle [Fig. 5(a)]; nearby particles were

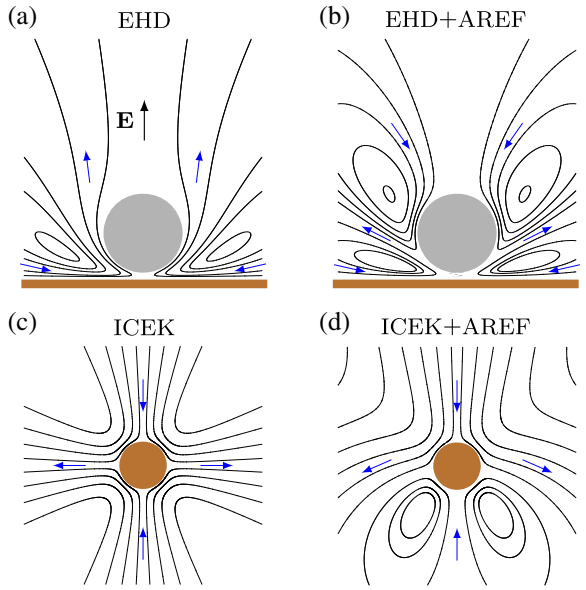

FIG. 5. Impact of AREFs on electrically induced fluid flows around (a) and (b) a charged nonconducting sphere near an electrode and (c) and (d) an isolated metallic cylinder. (See Supplemental Material [27] for streamline calculations).

mutually entrained in the flows, resulting in aggregation. Other workers noted, however, that the particle behavior depended sensitively on the type of electrolyte in the liquid [34–38]. Despite a great deal of experimental and theoretical investigation, there is still no consensus as to the mechanism underlying the electrolyte type dependence [38]. The existence of AREFs provides a new explanation: the flow field around each particle will be the superposition of the EHD flow generated on the electrode [39], and an electro-osmotic flow due to the steady AREF field generated on the particle surface. If the ionic mobility mismatch is sufficiently large, then the AREF-induced electro-osmotic flow dominates, and the resulting flow pattern will favor separation of nearby particles [Fig. 5(b), and Table S1 [27]].

Second, there are several unresolved aspects of "induced charge electrokinetics" (ICEK), a type of electrically driven fluid flow first elucidated in 2004 by Bazant and Squires [10,11] that triggered much research aimed at using applied electric fields to manipulate flow and objects in lab-on-a-chip devices [12,13]. The archetypal example of ICEK is the quadrupolar flow induced around a metallic cylinder in response to the applied field [Fig. 5(c)]. Scaling up this phenomenon for use as electrokinetic pumps in microfluidic devices, however, revealed experimental observations that ICEK theory fails to address [12,13,40]. Specifically, a reversal in fluid flow direction occurs at high frequencies; the standard ICEK theory predicts no such frequency effect. Similarly, the effect of ionic strength is unclear: fluid flows effectively cease at ionic strengths above 10 millimolar, again at odds with the theory. The existence of AREFs provides potential insight for both dilemmas. Taking the archetypal case of fluid flow around a conducting cylinder, the actual flow field will be the superposition of the ICEK flow and electro-osmotic slip along the cylinder surface due to the AREF [Fig. 5(d)]. Depending on the frequency and position of the cylinder, the AREF electro-osmotic velocity can dominate the flow pattern. Moreover, the AREF-induced slip velocity scales as c_∞^{-1} [cf. Fig. S5(b) [27]]. Therefore, any experiments aimed at elucidating the ionic strength dependence of ICEK would need to take into account the confounding effect of AREF-induced flows. More research is needed; the analysis presented here should serve as a starting point for consideration of the influence of AREFs in these and more complicated systems.

This material is based upon work supported by the National Science Foundation under Grant No. DMS-1664679.

*wdristenpart@ucdavis.edu
†grgmiller@ucdavis.edu

[1] A. D. Hollingsworth and D. A. Saville, J. Colloid Interface Sci. **257**, 65 (2003).
[2] P. J. Beltramo, R. Roa, F. Carrique, and E. M. Furst, J. Colloid Interface Sci. **408**, 54 (2013).
[3] C. Grosse and A. V. Delgado, Curr. Opin. Colloid Interface Sci. **15**, 145 (2010).
[4] A. S. Bandarenka, Analyst **138**, 5540 (2013).
[5] H. Wang, A. Thiele, and L. Pilon, J. Phys. Chem. C **117**, 18286 (2013).
[6] R. Hidalgo-Alvarez, A. Martln, A. Fernandez, D. Bastos, F. Martinez, and F. J. de las Nieves, Adv. Colloid Interface Sci. **67**, 1 (1996).
[7] R. Pusset, S. Gourdin-Bertin, E. Dubois, J. Chevalet, G. Meriguet, O. Bernard, V. Dahirel, M. Jardatab, and D. Jacobc, Phys. Chem. Chem. Phys. **17**, 11779 (2015).
[8] R. Pethig, Biomicrofluidics **4**, 022811 (2010).
[9] H. Zhao, Electrophoresis **32**, 2232 (2011).
[10] M. Z. Bazant and T. M. Squires, Phys. Rev. Lett. **92**, 066101 (2004).
[11] T. M. Squires and M. Z. Bazant, J. Fluid Mech. **509**, 217 (2004).
[12] M. Z. Bazant, M. S. Kilic, B. D. Storey, and A. Ajdari, Adv. Colloid Interface Sci. **152**, 48 (2009).
[13] T. M. Squires, Lab Chip **9**, 2477 (2009).
[14] M. Trau, D. A. Saville, and I. Aksay, Science **272**, 706 (1996).
[15] M. Trau, D. A. Saville, and I. A. Aksay, Langmuir **13**, 6375 (1997).
[16] S. Yeh, M. Seul, and B. I. Shraiman, Nature (London) **386**, 57 (1997).
[17] D. C. Prieve, P. J. Sides, and C. L. Wirth, Curr. Opin. Colloid Interface Sci. **15**, 160 (2010).
[18] C. S. Dutcher, T. J. Woehl, N. H. Talken, and W. D. Ristenpart, Phys. Rev. Lett. **111**, 128302 (2013).
[19] R. W. O'Brien and L. R. White, J. Chem. Soc., Faraday Trans. 2 **74**, 1607 (1978).
[20] E. H. B. Delacey and L. R. White, J. Chem. Soc., Faraday Trans. 2 **77**, 2007 (1981).
[21] W. B. Russel, D. A. Saville, and W. R. Schowalter, *Colloidal Dispersions*, 1st ed. (Cambridge University Press, Cambridge, England, 1991).
[22] E. J. Hinch, J. D. Sherwood, W. C. Chew, and P. N. Sen, J. Chem. Soc., Faraday Trans. 2 **80**, 535 (1984).
[23] C. S. Mangelsdorf and L. R. White, J. Chem. Soc., Faraday Trans. **93**, 3145 (1997).
[24] L. Hojgaard Olesen, M. Z. Bazant, and H. Bruus, Phys. Rev. E **82**, 011501 (2010).
[25] R. F. Stout and A. S. Khair, Phys. Rev. E **92**, 032305 (2015).
[26] O. Schnitzer and E. Yariv, Phys. Rev. E **89**, 032302 (2014).
[27] See Supplemental Material at http://link.aps.org/supplemental/10.1103/PhysRevLett.121.185504 for details of two-ion model, numerical solution, behavior of AREF near electrodes, AREF-induced forces and flows, streamlines calculations, effects of ionic strength and diffusivity on AREF, distribution of cation and anion in space and time, particle height bifurcation, and materials and methods, which includes Refs. [28–31].
[28] D. F. Martin and K. L. Cartwright, UC Berkeley, Report No. UCB/ERL M96/66, 1996 (unpublished).
[29] W. L. Briggs, V. E. Henson, and S. F. McCormick, *A Multigrid Tutorial*, 2nd ed. (Society for Industrial and Applied Mathematics, Philadelphia, 2000).

[30] G. Miller, *Numerical Analysis for Engineers and Scientists* (Cambridge University Press, Cambridge, England, 2014).
[31] Y. Solomentsev, M. Bohmer, and J. L. Anderson, Langmuir **13**, 6058 (1997).
[32] T. J. Woehl, B. J. Chen, K. L. Heatley, N. H. Talken, S. C. Bukosky, C. S. Dutcher, and W. D. Ristenpart, Phys. Rev. X **5**, 011023 (2015).
[33] S. C. Bukosky and W. D. Ristenpart, Langmuir **31**, 9742 (2015).
[34] J. Kim, J. L. Anderson, S. Garoff, and P. J. Sides, Langmuir **18**, 5387 (2002).
[35] J. D. Hoggard, P. J. Sides, and D. C. Prieve, Langmuir **23**, 6983 (2007).
[36] J. D. Hoggard, P. J. Sides, and D. C. Prieve, Langmuir **24**, 2977 (2008).
[37] C. L. Wirth, P. J. Sides, and D. C. Prieve, Phys. Rev. E **87**, 032302 (2013).
[38] T. J. Woehl, K. L. Heatley, C. S. Dutcher, N. H. Talken, and W. D. Ristenpart, Langmuir **30**, 4887 (2014).
[39] W. D. Ristenpart, I. A. Aksay, and D. A. Saville, J. Fluid Mech. **575**, 83 (2007).
[40] V. Studer, A. Pepin, Y. Chen, and A. Ajdari, Analyst **129**, 944 (2004).